

## **Wavelength dependence of the multiphoton ionization of CH<sub>3</sub>I by intense femtosecond laser pulses through Freeman resonances**

Ignacio M. Casasús<sup>a</sup>, María E. Corrales<sup>a</sup>, and Luis Bañares<sup>a,b\*</sup>

<sup>a</sup> Departamento de Química Física, Facultad de Ciencias Químicas, Universidad Complutense de Madrid, 28040 Madrid, Spain.

<sup>b</sup> Instituto Madrileño de Estudios Avanzados en Nanociencia (IMDEA Nanoscience), Cantoblanco, 28049 Madrid, Spain.

\* E-mail: lbanares@ucm.es

1. Photoelectron angular distributions (PEADs) that arise from a N-photon ionization process with linearly polarized light can be described by an expansion in spherical harmonics:

$$I(\theta) \approx \sum_{n=0}^{n=N} \beta_{2n} Y_{2n}(\theta) = \frac{\sigma}{4\pi} \sum_{n=0}^{n=N} \beta_{2n} \cdot P_{2n}(\cos(\theta)),$$

which corresponds to equation [6] of the main text. Here, we present the non-linear fitted coefficients obtained after the non-linear fitting of selected PEADs that are displayed in the text. The errors are computed as the standard deviations of the parameters and are shown in parentheses.

- a) From the experiments at 800 nm

Kinetic Energy (eV)	0.33	0.96	1.85	2.45
$\frac{\sigma}{4\pi}$	0,1914 (8)	0,2781 (10)	0,1201 (7)	0,0782 (7)
$\beta_2$	1,182 (7)	0,517 (8)	1,625 (10)	2,924 (10)
$\beta_4$	0,40 (1)	0,31 (1)	1,14 (1)	2,80 (1)
$\beta_6$	0,97 (1)	0,54 (1)	1,32 (1)	2,45 (1)
$\beta_8$	0,56 (2)	0,66 (1)	-0,06 (2)	1,74 (2)
$\beta_{10}$	0,33 (1)	-0,02 (2)	0,23 (2)	1,16 (2)
$\beta_{12}$	0,13 (2)	0,06 (2)	0,03 (2)	-0,11 (2)
$\beta_{14}$	0,04 (2)	0,00 (2)	-0,08 (3)	-0,06 (2)
$\beta_{16}$	-	-	0,09 (2)	-0,08 (2)

Table S1. Non-linear fitted coefficients of the PEADs observed at  $7.2 \text{ TW}\cdot\text{cm}^{-2}$ , shown in the Figure 5(a) of the main text.

Kinetic Energy (eV)	0.67	2.21	3.75
$\frac{\sigma}{4\pi}$	0,1828 (7)	0,1607 (7)	0,2247 (8)
$\beta_2$	0,921 (10)	0,825 (10)	0,630 (10)
$\beta_4$	0,81 (1)	1,08 (1)	0,66 (1)
$\beta_6$	0,93 (1)	1,38 (1)	0,57 (1)
$\beta_8$	1,36 (2)	0,50 (1)	0,51 (1)
$\beta_{10}$	0,04 (2)	1,10 (2)	0,15 (2)

$\beta_{12}$	-0.01 (2)	-0,18 (2)	0,53 (2)
$\beta_{14}$	-0.10 (2)	-0,01 (1)	-0,12 (2)
$\beta_{16}$	-	-0,03 (1)	-0,03 (2)

Table S2. Non-linear fitted coefficients of the PEADs observed at  $12.5 \text{ TW} \cdot \text{cm}^{-2}$ , shown in the Figure 5(b) of the main text.

Kinetic Energy (eV)	1.02	1.19	1.82
$\frac{\sigma}{4\pi}$	0,1760 (7)	0,1517 (8)	0,1635 (8)
$\beta_2$	1,099 (10)	1,344 (10)	0,664 (10)
$\beta_4$	1,06 (1)	1,41 (1)	0,79 (1)
$\beta_6$	0,76 (1)	1,07 (1)	1,26 (1)
$\beta_8$	0,82 (1)	1,05 (2)	0,41 (2)
$\beta_{10}$	0,59 (2)	0,63 (2)	0,66 (2)
$\beta_{12}$	-0,10 (2)	-0,05 (3)	0,07 (2)
$\beta_{14}$	-0,10 (2)	-0,13 (3)	-0,01 (3)
$\beta_{16}$	-0,06 (3)	-0,15 (2)	0,01 (3)

Table S3. Non-linear fitted coefficients of the PEADs observed at  $17.7 \text{ TW} \cdot \text{cm}^{-2}$ , shown in the Figure 5(c) of the main text.

b) From the experiments at 400 nm

Kinetic Energy (eV)	2.00	2.63	5.10	5.73
$\frac{\sigma}{4\pi}$	0,652 (3)	0,591 (3)	0,509 (5)	0,400 (6)
$\beta_2$	0,20 (1)	0,35 (1)	0,62 (4)	1,02 (4)
$\beta_4$	0,07 (2)	-0,08 (2)	-0,07 (4)	0,20 (4)
$\beta_6$	0,13 (2)	0,23 (2)	-0,13 (4)	-0,06 (4)
$\beta_8$	-0,05 (2)	-0,12 (2)	0,16 (5)	0,20 (5)
$\beta_{10}$	-	-	-0,03 (5)	-0,06 (5)

Table S4. Non-linear fitted coefficients of the PEADs observed at  $30.0 \text{ TW} \cdot \text{cm}^{-2}$ , shown in the Figure 9 of the main text.

c) From the experiments at 590 nm

Kinetic Energy (eV)	0.20	0.83	2.30	2.93
$\frac{\sigma}{4\pi}$	0,424 (1)	0,363 (2)	0,395 (2)	0,330 (4)
$\beta_2$	0,66 (1)	0,95 (1)	0,62 (1)	1,21 (1)
$\beta_4$	0,34 (1)	0,77 (1)	0,20 (1)	0,53 (1)
$\beta_6$	0,07 (1)	-0,20 (2)	-0,16 (2)	-0,15 (2)
$\beta_8$	0,04 (2)	0,10 (2)	-0,15 (2)	-0,49 (3)
$\beta_{10}$	-0,01 (2)	-0,02 (2)	0,08 (3)	0,12 (4)
$\beta_{12}$	-	-	0,05 (3)	-0,05 (4)

Table S5. Non-linear fitted coefficients of the PEADs observed at  $3.7 \text{ TW}\cdot\text{cm}^{-2}$ , shown in the Figure 12(a) of the main text.

Kinetic Energy (eV)	0.60	2.00	2.63	4.20	4.83
$\frac{\sigma}{4\pi}$	0,347 (2)	0,574 (2)	0,490 (2)	0,346 (3)	0,198 (3)
$\beta_2$	0,48 (1)	0,27 (1)	0,55 (1)	0,82 (1)	1,60 (1)
$\beta_4$	0,65 (2)	-0,18 (2)	-0,22 (1)	0,14 (1)	0,41 (1)
$\beta_6$	0,40 (2)	0,15 (2)	0,24 (2)	-0,01 (2)	0,01 (2)
$\beta_8$	0,18 (2)	-0,13 (2)	0,09 (2)	0,11 (2)	0,19 (3)
$\beta_{10}$	-0,03 (2)	0,01 (3)	-0,08 (2)	-0,06 (4)	0,07 (4)
$\beta_{12}$	-	-	-0,02 (2)	-0,01 (4)	-0,05 (4)

Table S6. Non-linear fitted coefficients of the PEADs observed at  $14.0 \text{ TW}\cdot\text{cm}^{-2}$ , shown in the Figure 12(b) of the main text.

2. Selected Abel-inverted photoelectron (PE) images obtained by photoionization of CH<sub>3</sub>I with femtosecond laser pulses in the visible range of the electromagnetic spectrum.

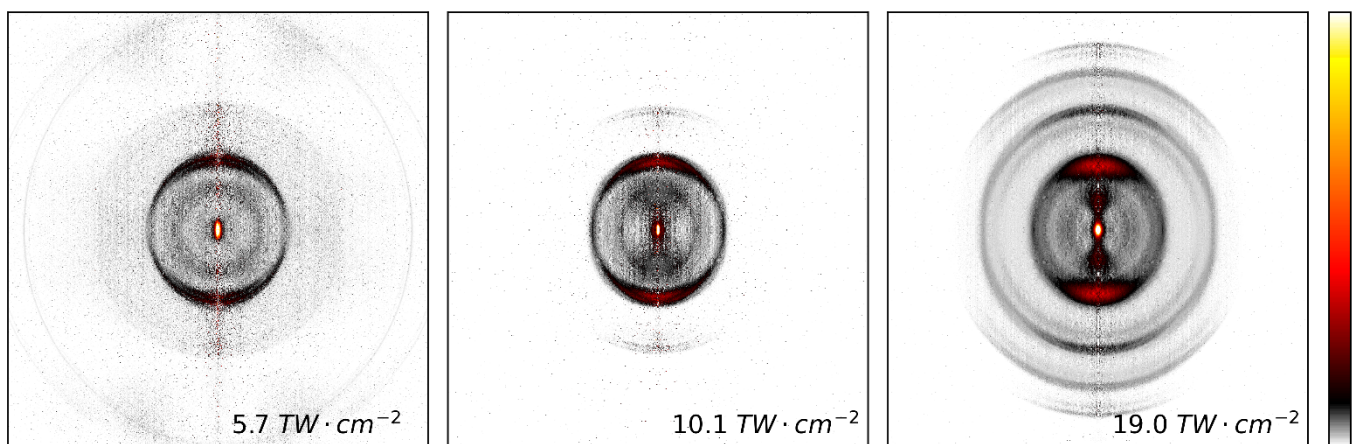


Figure S1. From the experiments performed at 575 nm.

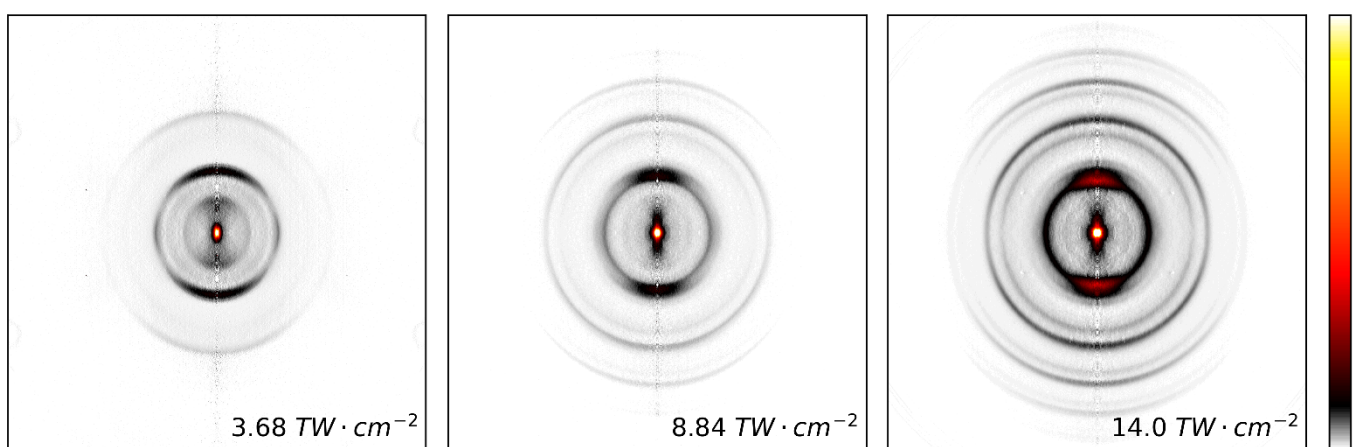


Figure S2. From the experiments performed at 590 nm.

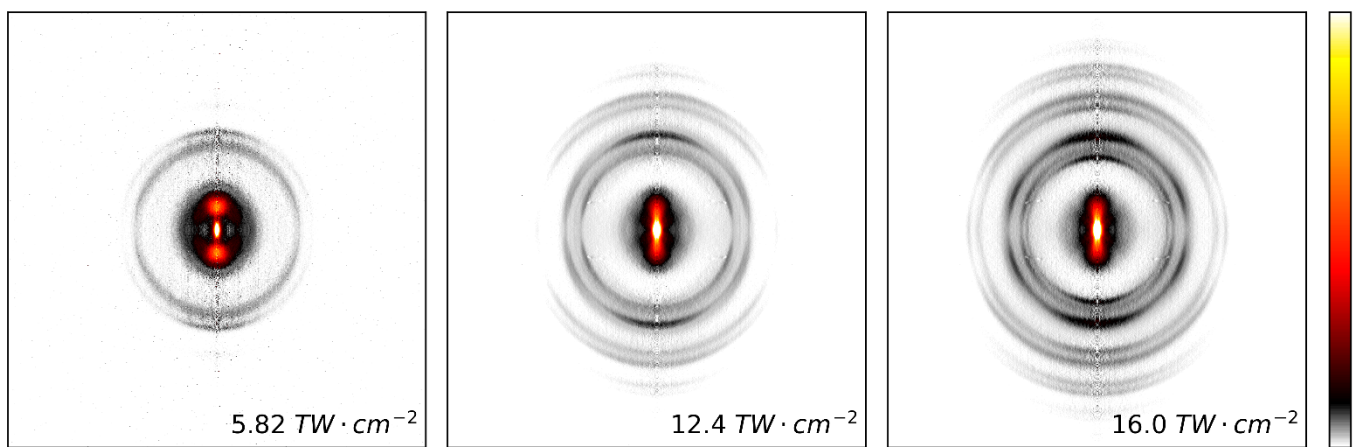


Figure S3. From the experiments performed at 630 nm.

3. Absolute laser intensity calibration of the visible experiments. In every Figure, (a) shows PEKDs obtained through angular integration of the Abel-inverted PE images. Laser intensity at which every distribution was obtained is written at their left, while ionization signal units are arbitrary and are normalized. Vertical dashed lines mark the position of selected signals in the distributions that are found. Lowercase letters label those signals, increasing the letter in the order of their increasing kinetic energy. (b) Presents the intensity-dependent radial distribution map of the previous PEKDs. Dotted lines represent the non-resonant ionization to the  $^2E_{1/2}$  ionic potential, while dashed lines to the  $^2E_{3/2}$  one. (c) Contains the intensity-dependent radial distribution of the intensity difference spectra map. Dotted lines represent the non-resonant ionization to the  $^2E_{1/2}$  ionic potential, while dashed lines to the  $^2E_{3/2}$  one.

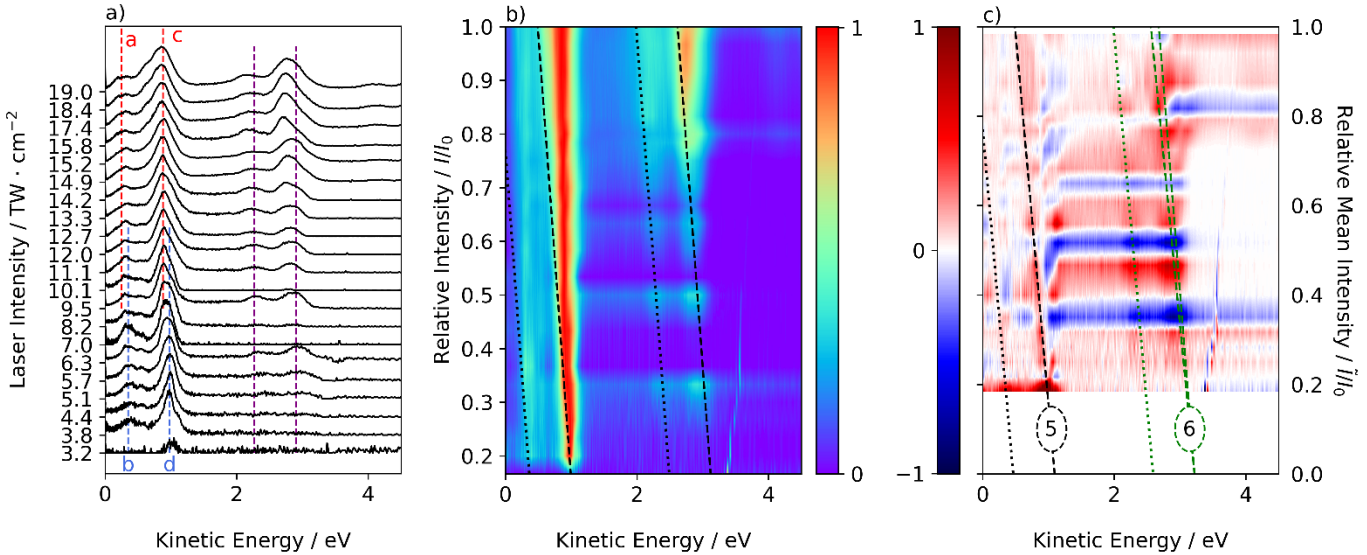


Figure S4. From the experiments performed at 575 nm. The slope of the ATI of order 6 (state  $^2E_{3/2}$ ) predicted by using  $I_0 = \pm 0.10 \cdot I_0$  is shown in green dashed lines, where  $I_0 = 19.0 \text{ TW} \cdot \text{cm}^{-2}$ .

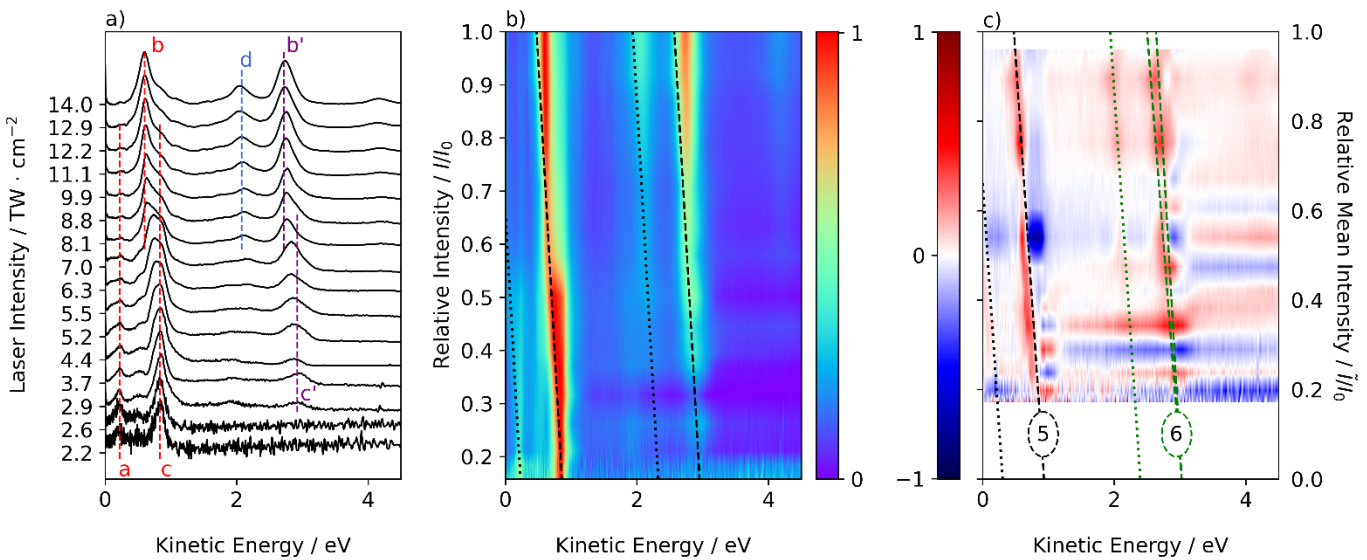


Figure S5. From the experiments performed at 590 nm. The slope of the ATI of order 6 (state  $^2E_{3/2}$ ) predicted by using  $I_0 = \pm 0.10 \cdot I_0$  is shown in green dashed lines, where  $I_0 = 14.0 \text{ TW} \cdot \text{cm}^{-2}$ .

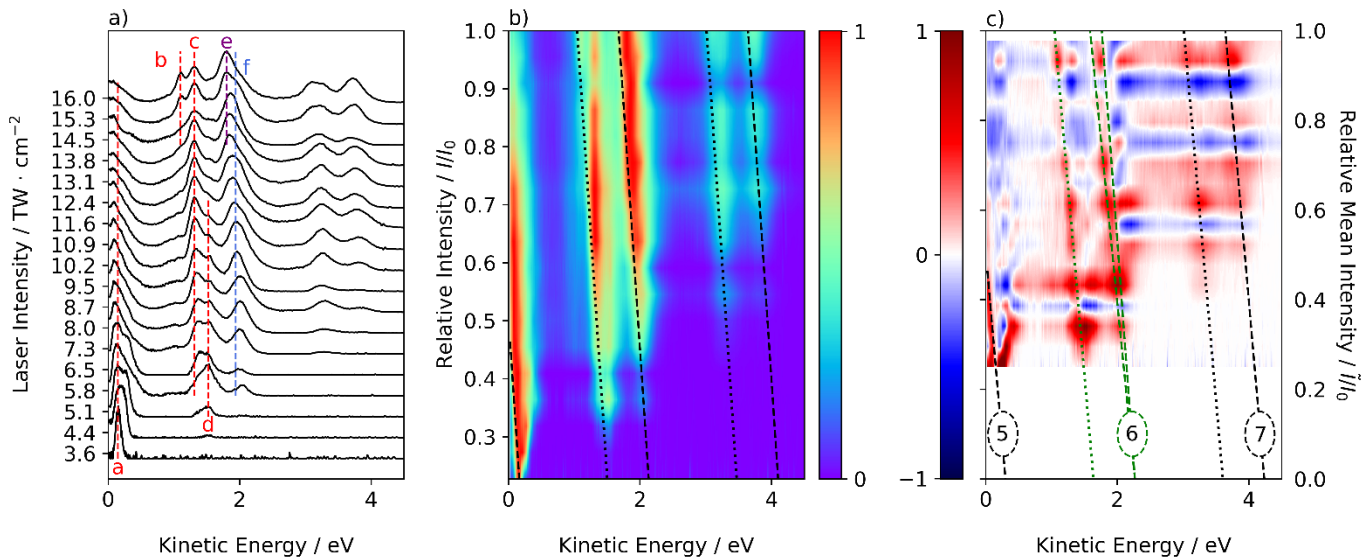


Figure S6. From the experiments performed at 575 nm. The slope of the ATI of order 6 (state  ${}^2\text{E}_{3/2}$ ) predicted by using  $I_0 = \pm 0.10 \cdot I_0$  is shown in green dashed lines, where  $I_0 = 16.0 \text{ TW} \cdot \text{cm}^{-2}$ .